

CHAPTER 5

TUNE MODULATION AND EXPERIMENT E778

Experiment E778, nonlinear dynamics in the Fermilab Tevatron, started in 1987 to answer several questions regarding nonlinear dynamics issues in accelerators, in particular how accurately the the linear aperture of an actual synchrotron compares to that predicted by design and simulation programs. Various types of simulation programs have been used within the field of accelerator physics, both to assist in machine design and lattice modification. These simulations are extremely important in the design of new accelerators such as SSC, LHC, and RHIC, where performance demands typically requiring magnets with larger apertures and higher field quality must be balanced against the financial burden of construction.

Examination of the linear aperture is a more straightforward matter than examining the dynamic aperture, defined as the betatron oscillation amplitude which separates stable motion from unstable motion over some period of time. The dynamic aperture depends on many quantities, such as the physical aperture of the machine and the time period over which stability is being questioned. The linear and dynamic apertures depend strongly on nonlinearities, both intentionally and unintentionally introduced, in the synchrotron; it is therefore important to be able to model these nonlinearities with confidence for the sake of reducing magnet cost without sacrificing performance, and design correction schemes for nonlinearities that adversely affect the performance of these machines.

Prior to 1991 several experimental runs of E778 investigated the linearity of the Tevatron in normal operational mode (i.e. without any intentionally introduced strong nonlinearities) and such effects as smear, detuning and dynamic aperture

as created by 16 controlled strong sextupoles. These portions of the experiment have been extensively documented elsewhere (Chao et. al. 1987b, Merminga 1989, Li 1990). Persistent signals due to resonant capture of a fraction of the beam were also used as an experimental beam diagnostic in E778, and comparison of kick amplitudes and persistent signal amplitudes allowed estimates of the island size δI .

In this chapter we describe the procedure and results of a tune modulation experiment performed in the Fermilab Tevatron in January, 1991. This experiment, a portion of Fermilab experiment E778, observed persistent signals in the horizontal transverse dimension corresponding to beam capture on a variety of resonances created by a set of strong sextupoles. The behavior of particles trapped in one of these resonances, the $5Q_x$ resonance at the horizontal tune $Q_x = 20.40$, was systematically examined under the influence of controlled tune modulation for two distinct nonlinear configurations and three different horizontal island amplitudes. For one particular case of sextupole configuration and island amplitudes a detailed analysis of the response of the persistent signal at high frequencies is found to agree with the one-dimensional tune modulation model presented in Chapter 4. A transverse diffusion experiment was also carried out during this experimental run but is not commented upon further here (Chen et. al. 1992).

The requirements for the E778 persistent signal and tune modulation experiment in the Tevatron are outlined in § 5.1. Preparations for the January, 1991 experimental run are described in § 5.2, including magnet calibrations and the results of preliminary tracking to determine which nonlinear magnet configurations should be used. The island tunes and detuning coefficients α are also measured from tracking of the configurations chosen for the experiment. The experimental run itself is described briefly in § 5.3, and in § 5.4 the data analysis procedure is explained and results of this experiment are summarized.

5.1 REQUIREMENTS FOR THE EXPERIMENT

Several requirements must be fulfilled before a persistent signal and tune modulation experiment can be undertaken. These requirements fall under two general categories: the requirements of the accelerator lattice and the requirements of the data acquisition system.

5.1.1 Lattice Requirements

The requirements of the machine lattice are threefold: first, the lattice must be relatively linear with the exception of strong controlled nonlinearities, which are used to create resonance islands in transverse phase space. Without a relatively linear machine, other sources of nonlinearity will affect the resonance under study, possibly changing its size and position in phase space. Although this does not invalidate the experiment, the results of particle tracking and theoretical predictions are much less likely to compare favorably with experiment in the presence of unknown strong nonlinearities. It has previously been demonstrated that the nominal configuration of the Tevatron is exceptionally linear (Chao et. al. 1987b). Several unused sextupoles originally intended for harmonic correction are ideal for use as controlled nonlinearities. The sixteen sextupoles shown in Figure (6.1) were chosen for use in this experiment.

The accelerator must have available a fast kicker magnet in the transverse plane under study. This kicker must have a kick time less than the revolution period of the accelerator in order to kick the beam only once. Typically most accelerators have fast kickers such as these for abort systems, injection and fast extraction. The Tevatron has several such kickers; the one chosen for this experiment is the horizontal proton injection alignment kicker which is located at the Tevatron lattice location E17 and has a fall time of approximately 1–2 μ s, much smaller than the 21 μ s revolution period of the Tevatron.

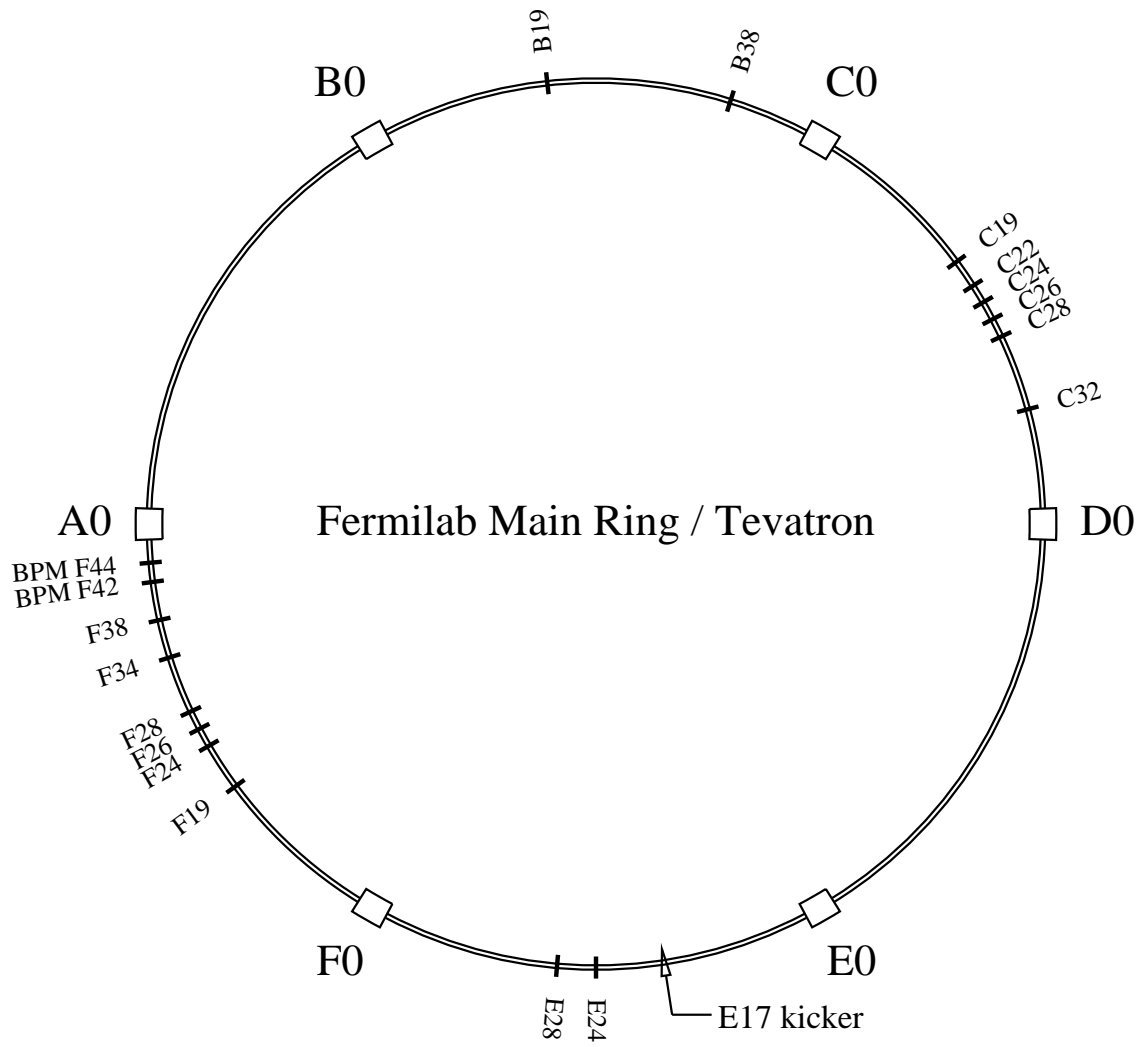


Figure 5.1: The lattice used in the January 1991 run of experiment E778, showing locations of sextupoles, beam position monitors and the E17 horizontal kicker.

To investigate tune modulation effects, the tune modulation parameters must be varied over wide ranges and controlled with a high degree of accuracy. Because the synchrotron frequency of off-momentum particles cannot be widely varied due to RF system considerations, using tune modulation produced by such oscillations is impractical. Instead a quadrupole or set of quadrupoles with low inductance can be powered sinusoidally, creating tune modulation directly. A set of quadrupoles exist in the Tevatron that are powered by a 720 Hz digital waveform; they are primarily used for fine adjustments during slow extraction for fixed target operation. These quadrupoles are described in more detail in Section 2.1 of this chapter.

There are other less unusual but no less important requirements for control of the accelerator lattice in this experiment. Linear coupling must be minimized, since this causes the coherent transverse oscillation produced by the kicker to couple into the unkicked plane. Chromaticity must be reduced to as small a value as possible, typically one or two units, so tune modulation induced by bunched beam synchrotron oscillations does not interfere with the controlled tune modulation of the modulated quadrupoles. These are both normal operational procedures in the Tevatron and can be easily be performed while on experimental shifts.

5.1.2 Data Acquisition Requirements

The data acquisition system used for E778 used is based on Sun CPU architectures, dual crates (both VME and Camac) and twin LeCroy 6810 5 MHz 12-bit transient digitizers. It is diagrammed in Figure (5.2). The data acquisition system requires three inputs from the central accelerator control system: a turn-by-turn clock used to gate the turn-by-turn digitizers (which must be appropriately synchronized to the kicked bunch), a trigger to start the digitizing process, and the BPM signals themselves. The general configuration as a simple portable unix-based data acquisition system was originally implemented as MIRABILE at

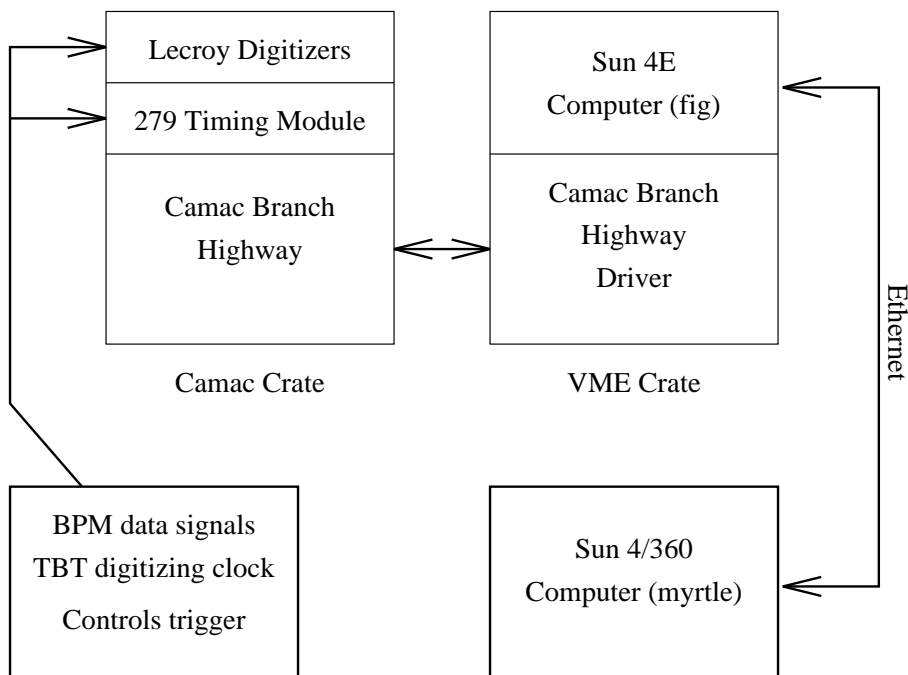


Figure 5.2: A block diagram of the E778 data acquisition system, showing both VME and Camac crates, general networking, and input signals.

Fermilab and the Cornell Electron Storage Ring (CESR) (Peggs, Saltmarsh and Talman 1987).

The turn-by-turn clock was supplied by the RF clock of the Tevatron divided by 1113, since there are 1113 RF cycles in one revolution of the machine when the 53 MHz bunching RF is on. A programmable delay to synchronize this clock with the kicked bunch was created by a Fermilab Camac 279 module which delays in increments of 7 RF cycles. The acquisition trigger was supplied by a programmable 345 card synchronized to a timing event in the Tevatron timeline, allowing data acquisition either to begin on the order of thousands of turns before the E17 kicker was fired, allowing observation of decoherence for detuning measurements, or hundreds of thousands of turns after the kick, when transients had damped and

the only coherent oscillation still remaining was the persistent signal.

The beam position monitor signals were acquired from the voltage difference of individual plates of parallel plate horizontal BPMs at the F42 and F44 Tevatron locations. Front-end hardware included a peak-detector and a pulse stretcher with a decay time on the order of several microseconds. This setup gives output signals which are appropriate for digitization by the Lecroy 6810 digitizers. For the frequency-domain data analysis presented later in this chapter, note that full phase space reconstruction is not necessary and so only one digitized BPM signal, from F42, was used in this analysis.

A significant amount of software development also was needed for this project. The entire set of data acquisition system software was developed in C and C++ using the tools of ISTK (the Integrated Scientific Toolkit) developed by Chris Saltmarsh, Vern Paxson and others (Lutz 1991). The data transfer protocol of ISTK is SDS, the self-describing data standard which allows storage of all turn-by-turn data in simple processor-portable form. ISTK also includes a sequencing language and executive, Glish, which allows the control of many dependent tasks, or agents. For E778 there were several of these agents, including Camel (the Lecroy 6810 control program), Harc (the data archiver), Soc (the main experiment user interface) and Clod (the delay controller for the Camac 279 delay module). The Glistk graphics library, developed on top of the native C++ window management system InterViews, was used to write graphical user interfaces for all of these programs. A sample user interface for Camel is shown in Figure (5.3) with typical digitizer settings for the January 1991 E778 run.

5.2 LOCAL PREPARATION FOR THE EXPERIMENT

5.2.1 Magnet and Kicker Calibration

camel			
Branch 0	Crate 1	Station 6	Reset BCS
<input checked="" type="checkbox"/> Real Time Write ON		WRITE ALL	
CAMEL SETTINGS		MODULE	
camel_6		BZ Z C <input checked="" type="checkbox"/> I <input checked="" type="checkbox"/>	
<input checked="" type="checkbox"/> Editable <input type="checkbox"/> SWAP		Arm / DisArmed	
TRIGGER		<input checked="" type="checkbox"/> LAM Disabled	
<input checked="" type="checkbox"/> No Holdoff		Lock Retry 64	
Time Stamp Res 10 msec		Module Unlocked	
Source External		TIMEBASE	
Slope Positive		<input checked="" type="checkbox"/> Single Timebase	
Coupling DC		f1 External f2 50 Hz	
Upper Level 160		MEMORY	
Lower Level 0		Block 8 K Samp 128 K	
Post Trigger 4		Segments 1	
Delay 0		CHANNELS	
1 on	2 on	4 on	
			Full Scale Offset Coupling
<input checked="" type="checkbox"/> 1	H F44	2.048 V	128 AC Diff
<input checked="" type="checkbox"/> 2	H F46	2.048 V	128 AC Diff
<input checked="" type="checkbox"/> 3	V F43	2.048 V	128 AC Diff
<input checked="" type="checkbox"/> 4	V F45	2.048 V	128 AC Diff
DATA FLOW			
READ FROM CAMAC		<input type="checkbox"/> Manual Arm	
SHIP		<input type="checkbox"/> Manual Stop	
INITIALIZE		<input type="checkbox"/> No Link	
RESET		Archive File: DefaultFile	
			
X	Q	InstaQuit	

Figure 5.3: Camel, the graphic user-interface and control program for a Lecroy model 6810 digital waveform recorder. Settings are typical for those used in the January 1991 run of experiment E778.

Configuration	Sextupoles							
	E24	F19	F24	F34	B19	C19	C22	C24
	E28	F26	F28	F38	B38	C26	C28	C32
91_0	+/-	+/-	-/+	+/-	0	+/-	+/-	+/-
91_1	0	+/-	+/-	-/+	0	+/-	+/-	-/+
91_2	+/-	+/-	+/-	-/+	0	+/-	+/-	-/+

Table 5.1: Sextupole polarities and locations for 1991 E778 configurations. The first sign indicates the polarity of the first listed sextupole in each column. All sextupoles used in the actual tune modulation experiment were driven at a current of 30 amperes.

Knowledge of the sextupole strengths and their variation with current is crucial. Experimental results cannot reasonably be expected to match those of particle tracking if the strengths and locations of the strong nonlinearities are not known accurately and if other sources of nonlinearity are not accounted for.

Calibration measurements performed before the sextupoles were installed measured a magnetic field of $B_s = 0.148$ T at $r = 1$ inch from the magnet center; the sextupoles also have length $L_{sex} = .732$ m. Using the magnetic rigidity $|B\rho| = 500$ T-m for the Tevatron at its injection energy of 150 GeV where the experiment was performed gives the normalized sextupole strength of the sextupoles used at a current of 50 amperes:

$$\tilde{b}_2 = \frac{B_0 L}{|B\rho|} b_2 = \frac{B_s L}{|B\rho| r^2} = 0.336 \text{ m}^{-2} . \quad (5.1)$$

During the actual run the sextupole currents used were 30 Amps, with a corresponding normalized sextupole strength of $\tilde{b}_2 = 0.201 \text{ m}^{-2}$.

The sextupoles are also ganged together on 9 separate buses, paired with opposite polarities as listed in Table (5.1) with the exception of the B19 and B38 sextupoles which are individually powered. The configuration 91_0 listed in this table is the nominal operational configuration, and this configuration and 91_1 were those investigated in the actual tune modulation experiment. A decision

was made to turn off the B19 and B38 sextupoles to limit the number of configurations investigated in preliminary tracking.

The QXR quadrupoles used for tune modulation were also calibrated before the experimental run, and again during the initial startup shifts. These quadrupoles are driven by a digital waveform generated with a clock rate of 720 Hz, so they can modulate the tune at frequencies up to 360 Hz or $Q_M = 7.55 \cdot 10^{-3}$. Calibration was performed at DC current to measure the variation in tune versus quadrupole current, and showed the expected linear response in Figure (5.4), giving the tune changes

$$\begin{aligned}\Delta Q_x &= 4.1 \cdot 10^{-4} I_Q , \\ \Delta Q_y &= -1.0 \cdot 10^{-4} I_Q ,\end{aligned}\tag{5.2}$$

where I_Q is the quadrupole current in amperes. For the QXR system a current of 5 amperes was provided by a current supply for 1 volt setting on the control system, and the current range for this supply was 0 to 50 amperes. For a maximum modulation amplitude of 25 amperes or $q = 1.02 \cdot 10^{-2}$, a constant current was of 25 amperes was superimposed on the sinusoidal modulation when the QXR system was used.

AC calibration of the QXR system is significantly more difficult, since tune measurements currently cannot be acquired more quickly than once or twice per second in the Tevatron. A calibration of the QXR quadrupoles was instead performed by setting the voltage on the voltage source to a certain value with a sinusoidal modulation with an amplitude of 5 amperes and observing the read-back of the actual current supplied to the quadrupoles. This procedure allows measurement of the inductive decay of quadrupole response with rising frequency, showing a hyperbolic rolloff beginning near 100 Hz as in Figure (5.5). This measurement was performed during Tevatron downtime without making physical measurements of tune changes on the actual beam.

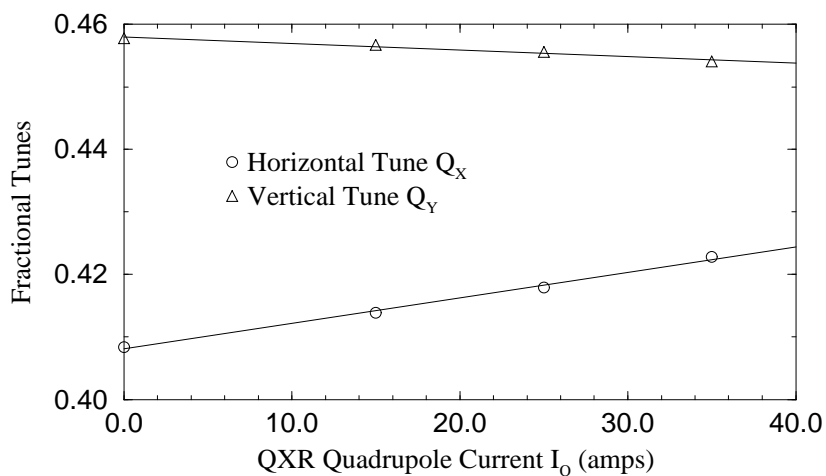


Figure 5.4: DC QXR quadrupole calibration, showing horizontal and vertical tune versus quadrupole current I_Q . Linear fits give $\Delta Q_x = 4.1 \cdot 10^{-4} I_Q$ and $\Delta Q_y = -1.0 \cdot 10^{-4} I_Q$.

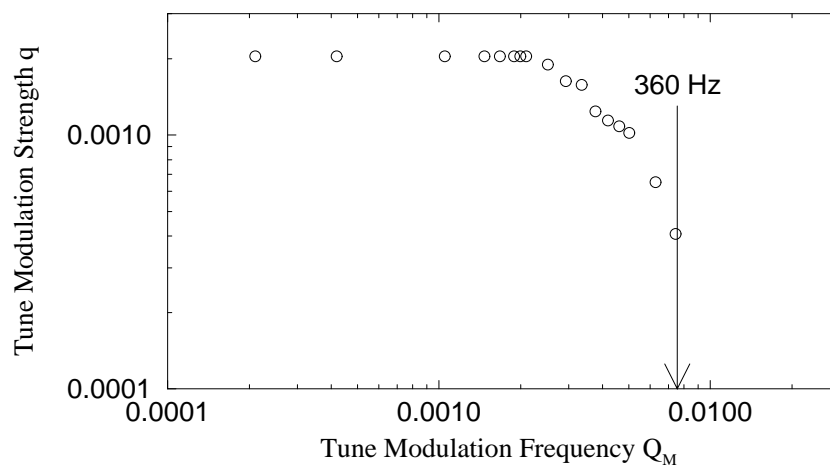


Figure 5.5: AC QXR quadrupole calibration, performed at 5 amps excitation current corresponding to tune modulation strength $q = 2 \cdot 10^{-3}$. Response rolloff begins at 100 Hz, or a tune modulation frequency of approximately $Q_M \approx 2 \cdot 10^{-3}$.

There is some concern about the effects of skin depth and penetration into the stainless steel beam pipe of the Tevatron by the field of the QXR quadrupoles. The conductivity of this material is approximately $\sigma = 4 \cdot 10^7 \text{ (ohm m)}^{-1}$, giving a skin depth of approximately 4 mm at frequencies of 350 Hz. This is several times the actual thickness of the beam pipe in the Tevatron, approximately 1.5 mm, and so for all frequencies involved in the chirp there should be negligible damping of the quadrupole modulation amplitude by conductive effects of the beam pipe.

5.2.2 Preparatory Tracking and Simulations

Once the sextupole strength scaling versus excitation current is known, tracking can be performed to find the optimal conditions for beam capture in a resonance island. The transverse phase space should contain large resonance islands, similar to those pictured in Figure (3.1). These resonance islands should not be severely distorted by the presence of the $3Q_x$ resonance, which is driven to first order by the sextupoles — previous E778 runs have measured such distortions (Chao et. al. 1987b, Merminga and Ng 1992). The resonance islands should also have fixed point phases positioned in such a manner that a stable fixed point lies in the x' direction of the phase space at the E17 kicker; this maximizes the amount of beam captured in the resonance island and the persistent thus produced. And finally, tracking should predict island tunes that fall within the experimentally accessible range for the tune modulation experiment.

Beta functions and phase positions of the sextupoles and E17 kicker were found using the most recent version of the Tevatron lattice and the accelerator design code MAD 8.1. A lattice was designed in Evol using only the sextupoles and linear phase advances, and the phase space at the kicker for a variety of configurations was produced. Of several configurations investigated, the configurations 91_1 and 91_2 satisfied the above criteria, as well as the nominal configuration 91_0. During

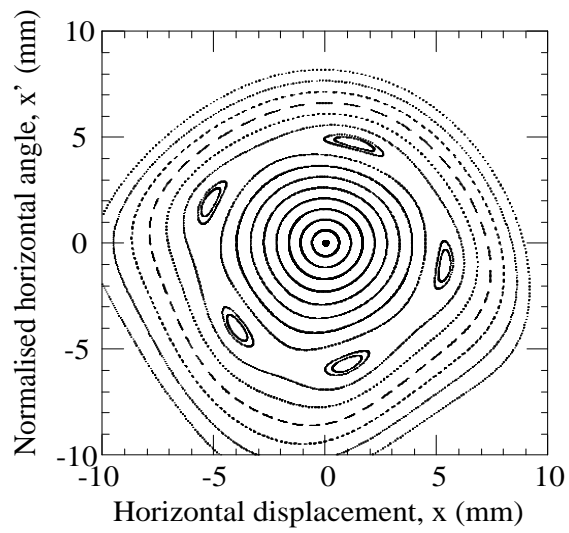


Figure 5.6: Transverse phase space for the 91_0 sextupole configuration at the E17 kicker. Tracking was performed with Evol with base tunes $(Q_x, Q_y) = (20.394, 20.460)$.

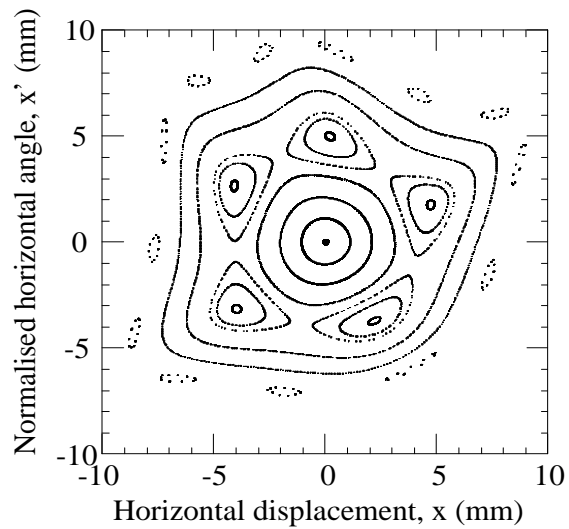


Figure 5.7: Transverse phase space for the 91_1 sextupole configuration at the E17 kicker. Tracking was performed with Evol with base tunes $(Q_x, Q_y) = (20.406, 20.460)$.

the experimental run only configuration 91_1 and the nominal configuration 91_0 were investigated.

Figures (5.4) and (5.5) show the phase spaces produced by the 91_0 and 91_1 sextupole configurations, respectively. Each has a separate variation of tune with amplitude, necessitating different base tunes for these phase space diagrams in order to detune into the resonance and display resonance islands, and both show resonance islands that are positioned properly without severe distortion from the presence of the third-integer resonance. The island tunes for each of these sextupole setups are 335 Hz ($Q_I = 7 \cdot 10^{-3}$) and 700 Hz ($Q_I = 1.9 \cdot 10^{-2}$) respectively, indicating that the resonant region should be barely accessible for lattice 91_0, but not for lattice 91_1. There are also small $13Q_x$ resonance islands evident in the phase space of the simulated 91_1 lattice, indicating that capture on resonances other than the $5Q_x$ is feasible in these configurations.

5.3 THE EXPERIMENTAL RUN

The experimental run of this section of E778 took place during two weekends in January, 1991, lasting a total of fourteen eight-hour shifts. Of those shifts, nearly a third each were dedicated to setup, the diffusion experiment and the persistent signal and tune modulation experiment.

Shifts for the first weekend were dedicated to debugging and testing the data acquisition system, calibrating and testing tune modulation quadrupoles, and scanning various kicker voltages, base tunes and nonlinearity configurations to find persistent signals. For this section of the weekend, the data acquisition system acquired 64 kiloturns of data, or approximately 1.4 seconds of data per data-taking “shot”. Persistent signals were located at $Q_x = 0.375$ (the $8Q_x$ resonance), $Q_x = 0.400$ (the $5Q_x$ resonance), and $Q_x = 0.417$ (the $12Q_x$ resonance). The E17 kicker kick amplitude was also calibrated versus applied kicker voltage in the

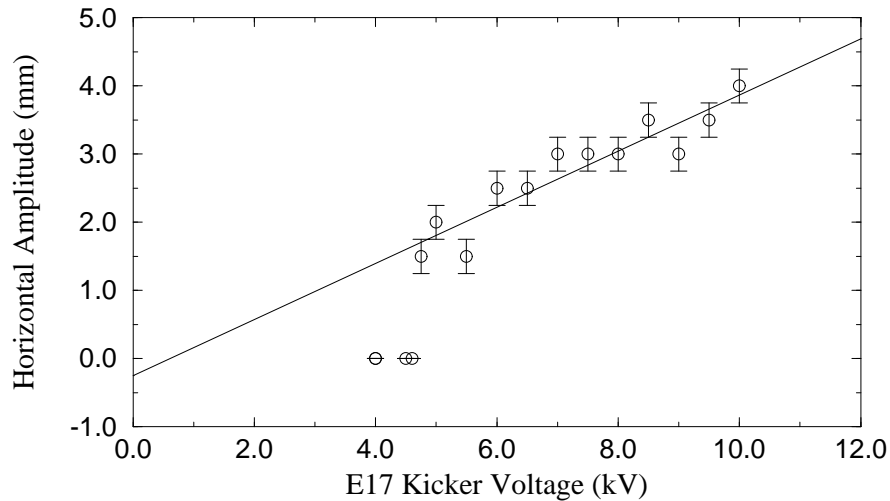


Figure 5.8: Calibration of the E17 kicker voltage versus kick amplitude. The linear fit slope is 0.41 mm/kV, and the kicker does not fire at voltages below 4.75 kilovolts.

early portion of the run; response was found to be approximately linear, with a .41 mm/kV slope. Samples of the turn-by-turn data produced online by the data acquisition system are shown in Figures (5.9) and (5.10), showing both a resonant persistent signal and gaussian decoherence without beam capture:

The event timeline for a typical 2 minute machine cycle or “shot” was as follows:

- Inject beam into Tevatron at 150 GeV, without acceleration, and coalesce to single bunch. (0–7 seconds)
- Reduce normalized beam emittance from 15π mm–mrad to 3π mm–mrad with scraper at Tevatron lattice location D17 (10–30 seconds)
- Ramp up sextupole currents and trigger E17 kicker. (35–45 seconds)
- Wait approximately 10 seconds for transients from the transverse kick to settle. (45–56 seconds)
- Trigger data acquisition system and tune modulation quadrupoles. (56–58 seconds)
- Data transfer, sextupole ramp down and preparation for the next

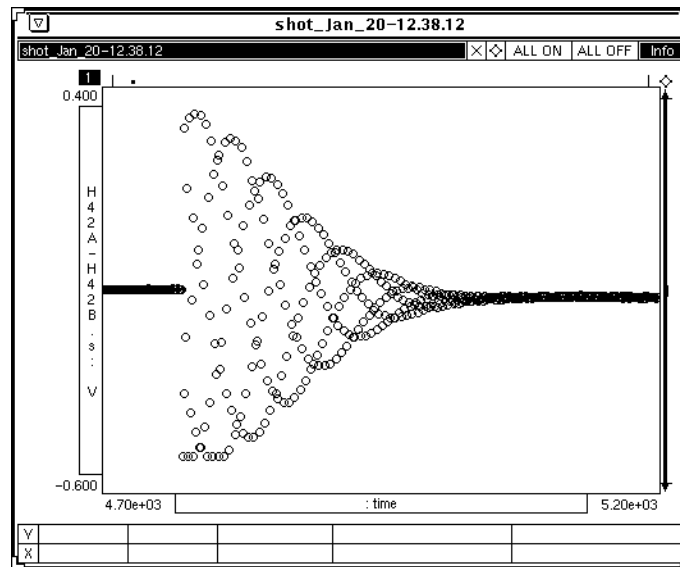


Figure 5.9: Sample turn-by-turn data at kick time, showing the kick and gaussian decoherence. Kicker voltage is 11 kV, and the lattice is 91.0; graphics are produced by the kaspar graphics program.

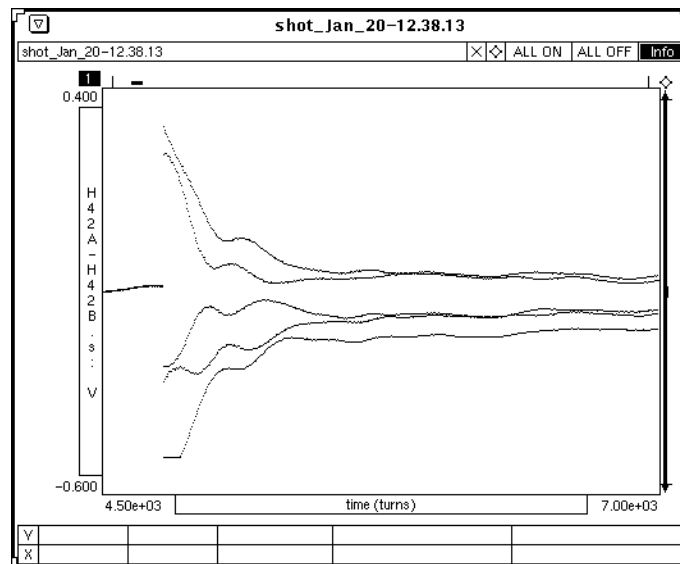


Figure 5.10: Sample turn-by-turn data at kick time, showing the kick and production of a $Q_x = 20.40$ persistent signal. Kicker voltage and lattice are as in above figure.

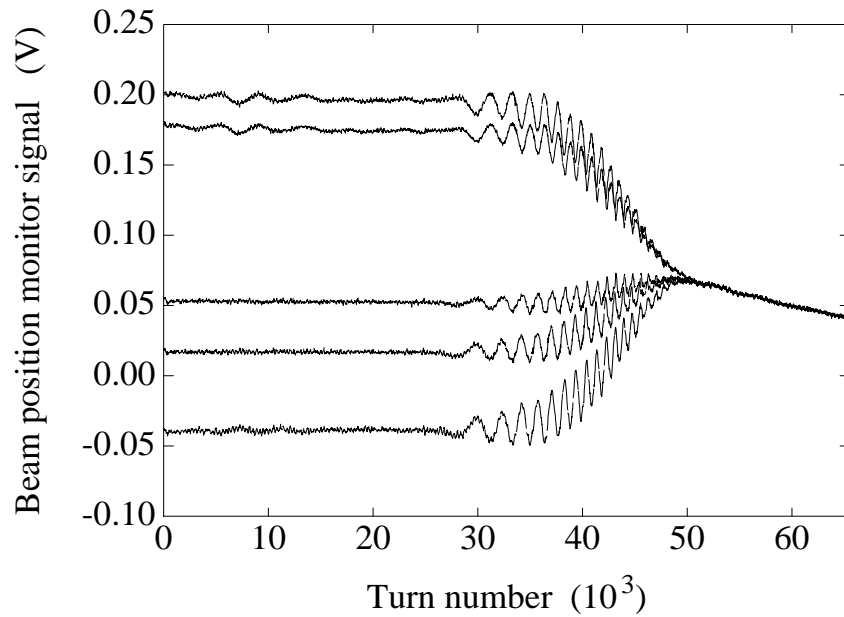


Figure 5.11: Turn-by-turn data for a strong persistent signal destroyed by chirped tune modulation. The tune modulation strength and frequency were ramped from $(q, Q_M) = (0, 0)$ to $(1.0 \cdot 10^{-2}, 3.1 \cdot 10^{-3})$. Lattice configuration is 91_0.

shot. (60-120 seconds)

Some unsystematic tune modulation data were also acquired in the first weekend for the nominal 91_0 lattice, starting approximately 9 kiloturns after the data acquisition system was activated and ramping for one second, or 47.7 kiloturns. An excellent example of the turn-by-turn data thus produced is shown in Figure (5.11) where the tune modulation parameters are chirped from $(q, Q_M) = (0, 0)$ to $(1.0 \cdot 10^{-2}, 3.1 \cdot 10^{-3})$. At approximately 28 kiloturns amplitude modulation of the islands becomes clearly visible, and the resonant response of the system destroys the persistent signal between 35 and 45 kiloturns.

On the second weekend systematic tune modulation scans were performed in order to make the search of the available tune modulation parameter space more efficient. For QXR voltages ranging roughly logarithmically from 0.1 volts to 5

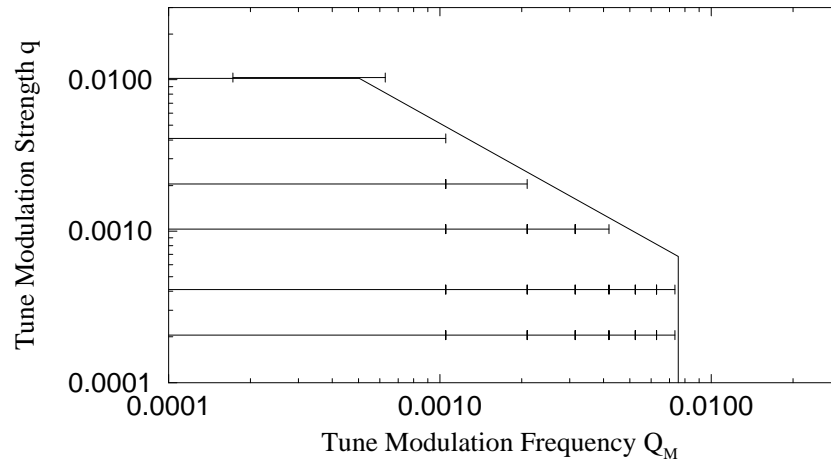


Figure 5.12: Distrubution of systematic tune modulation scans.

volts ($q = 2 \cdot 10^{-4}$ to 10^{-2}), chirps were performed in 50 Hz segments within the region of linear quadrupole response. During this second weekend such scans were performed for two kick amplitudes (5 kV and 9 kV) with the 91_1 configuration, and two kick amplitudes (7 kV and 9 kV) in the 91_0 configuration, all concentrating on the $5Q_x$ resonance. Some individual chirps ranging from 0 to 350 Hz were also performed at small modulation amplitudes. Upgrades to the data acquisition system also allowed digitization of 128 kiloturns of data per shot, approximately 2.7 seconds of real beam time.

5.4 DATA ANALYSIS AND RESULTS

Approximately one gigabyte of turn-by-turn data were taken in the January 1991 run of E778. This included both turn-by-turn data taken at kick time away from a resonance to measure the variation of tune with amplitude by decoherence, and turn-by-turn data taken after initial transients had decayed and tune modulation was turned on. This section describes the analysis of both the detuning and tune modulation data.

5.4.1 Measuring Detuning

Previous results from E778 and elsewhere have observed and successfully compared measurements of the decoherence of a gaussian beam kicked transversely into sheared nonresonant phase space with theory (Chao et. al. 1987b, Merminga 1989, ByrdThesis). For a gaussian beam of transverse size σ_x kicked to produce a coherent oscillation of amplitude $X_0 \gg \sigma_x$ as observed at a beta function of β_{obs} , the decoherence of the observed centroid position is predicted to be approximately gaussian (Chao et. al. 1987a):

$$x(t) \approx X_0 \exp \left[-\frac{1}{2} \left(\frac{2\pi\sigma_x\alpha X_0 t}{\beta_{obs}} \right)^2 \right], \quad (5.3)$$

where α is the one-dimensional Hamiltonian detuning from Equation (3.7).

The analysis program Tevex developed by Peggs, Chen and Merminga (Merminga 1989) was used to fit turn-by-turn data from two horizontal BPMs to the predicted gaussian decoherence. Tevex uses a five-parameter fit: the exponential term in the gaussian decoherence, values for the closed orbit offsets (or digitizer voltage offset) at both BPMs, the phase advance between the BPMs and the ratio of the horizontal beta functions at the BPMs. Tevex also returns the horizontal tune and the horizontal smear. Two approaches can be taken to measure the detuning parameter α : if the beam size and the beta functions at the BPMs are accurately known, the fit of the gaussian decoherence exponent by Tevex gives the detuning. However, if these are not known but the base tune setting of the machine is, then one can calculate from the tune returned by Tevex how much the tune has shifted for a given kick and thus the detuning. This second procedure was the procedure followed here, though the former method returns similar detuning after substitution of a typical beam size and beta function.

Figures (5.13) and (5.14) display a comparison of the detuning data for both nonlinear configurations examined to tracking with Evol through these configu-

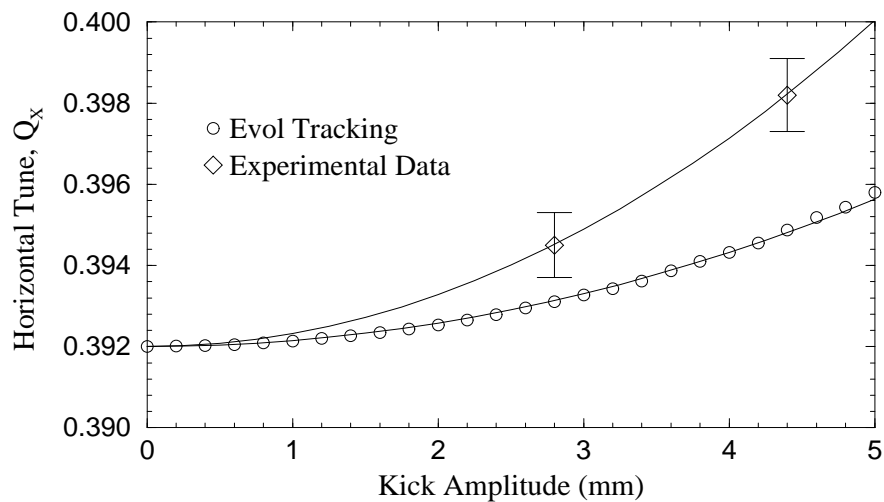


Figure 5.13: Comparison of Evol tracking to detuning data for the 91_0 sextupole configuration.

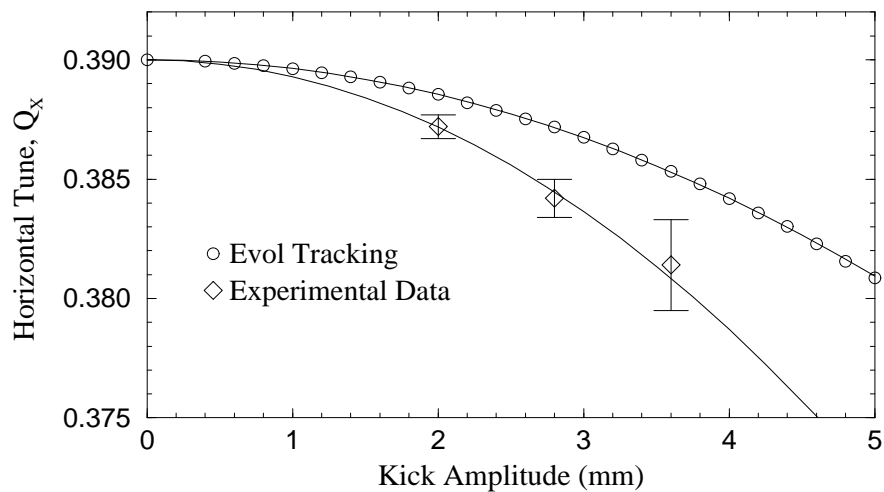


Figure 5.14: Comparison of Evol tracking to detuning data for the 91_1 sextupole configuration.

rations, with lines displayed as fits to each set of data. The evident discrepancy between tracking and experiment can be due to several different factors. The base tune setting of the Tevatron was noted during the course of the run to be rather inaccurate, varying by as much as 0.005 units from set values. Allowing this base tune of the experimental measurement to vary by this amount provides a better fit of the detuning. The sextupole strengths used in tracking may also differ by those experimentally used; since the detuning is driven to second order in sextupole strength, a difference by a factor of 1.4 between simulated and experimental sextupole strengths is sufficient to reconcile the detuning as shown in these figures.

5.4.2 Frequency Domain Behavior

Because the boundaries between regions in the tune modulation stability plane (q, Q_M) scale with the island tune, Q_I , it is logical to expect the frequency response of the beam to give information about the rate at which the phase-locked portion of resonance island is shrinking in response to chirped tune modulation. A fast Fourier transform (FFT) applied to a segment of unmodulated persistent signal turn-by-turn data displays an extremely sharp peak at exactly the resonant tune due to the highly coherent nature of the island-to-island motion that occurs for trapped particles. As particles are lost from this coherent signal due to tune modulation, the amplitude of this peak in the FFT spectrum decays with a rate that indicates how quickly the stable portion of the resonance island is shrinking.

For a 128 kiloturn data set acquired during the second weekend, the data was partitioned into overlapping 8192 turn segments, and FFTs were performed. This gives a frequency resolution in the resulting power distribution of approximately 10^{-4} for each FFT. The amplitude of these FFTs were then plotted versus time.

The three-dimensional plots of FFT amplitude versus frequency within the FFT

and turn number are displayed in Figure (5.15) through (5.22), for the configuration 91_0, a kicker voltage of 9 kV, the smallest modulation amplitude $q = 2 \cdot 10^{-4}$ and both 50 Hz and 350 Hz frequency chirps. These diagrams all have a large spike exactly at the resonant frequency, 0.4, which corresponds to the persistent signal — as the modulation detraps particles from the resonance island, this persistent signal decays. Progressing through the 50 Hz chirps, the persistent signal lifetime under modulation decreases steadily until the chirp from 300 Hz to 350 Hz. The stability of this scan indicates that the island frequency has been passed by the modulation frequency, thus implying that the island tune to be somewhere between 250 Hz and 300 Hz. For both configurations and sets of kicks examined, these are the only such data to exhibit behavior that indicates stability above the island frequency. We therefore discuss in the following how the island tune can be found more accurately from this data.

A convenient way to view this decay is by examining the instantaneous decay rate of the persistent signal from FFT to FFT, or as time (and the modulation frequency) increases. Assume that this decay is exponential and of the form

$$A_{\text{FFT}}(t) = A_0 e^{-\gamma t} , \quad (5.4)$$

where A_0 is the initial FFT amplitude and γ is the instantaneous persistent signal decay rate expressed in inverse turns. This gives a formula for the decay rate between any two times t_1 and t_2 :

$$\gamma = \frac{\log A_{\text{FFT}}(t_1) - \log A_{\text{FFT}}(t_2)}{t_2 - t_1} . \quad (5.5)$$

One particular advantage of this analysis is that it is independent of the initial Fourier amplitude A_0 . If the BPM voltage varies linearly with centroid position, such an approach in the frequency (or tune) domain does not require scaling for variations in beam current from shot to shot or fraction of the beam captured.

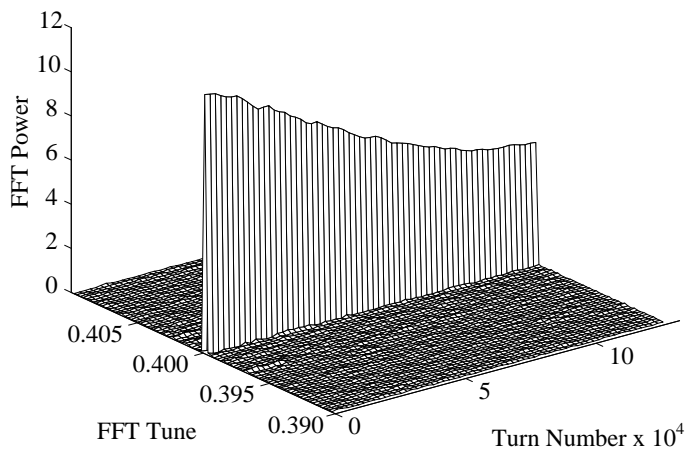


Figure 5.15: A segmented FFT for turn-by-turn tune modulation of the 91.0 sextupole configuration. Here $q = 2 \cdot 10^{-4}$ and Q_M is chirped from 0 to 50 Hz. Overlapping FFTs are taken every 8192 turns, and the amplitude of these FFTs for the frequency range (0.398, 0.402) is displayed versus turn number, or modulation frequency during the chirp.

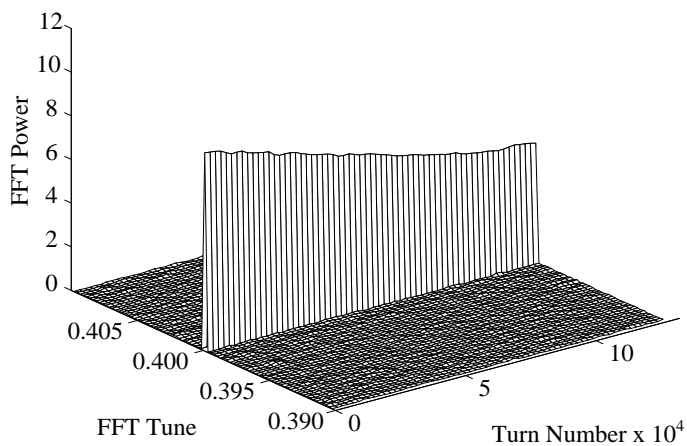


Figure 5.16: Same as Figure 5.15, with Q_M chirped from 50 to 100 Hz.

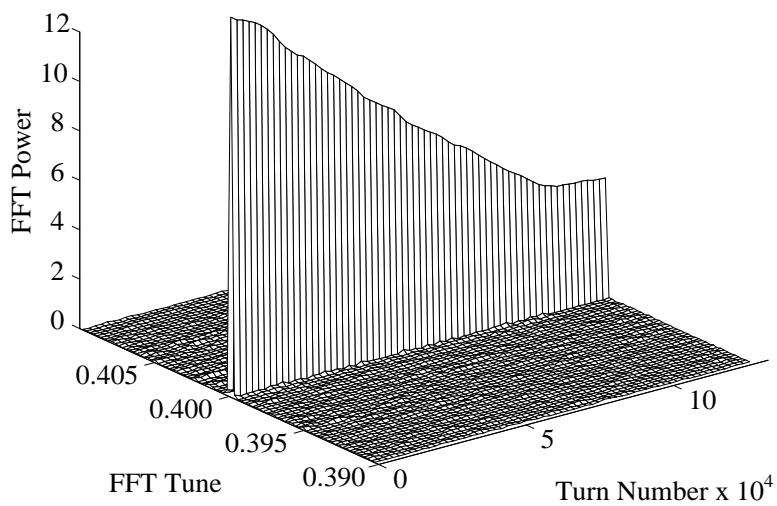


Figure 5.17: Same as Figure 5.15, with Q_M chirped from 100 to 150 Hz.

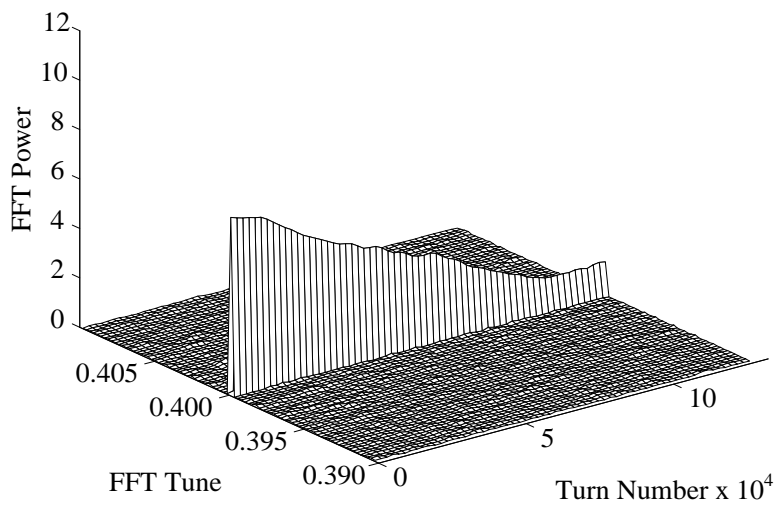


Figure 5.18: Same as Figure 5.15, with Q_M chirped from 150 to 200 Hz.

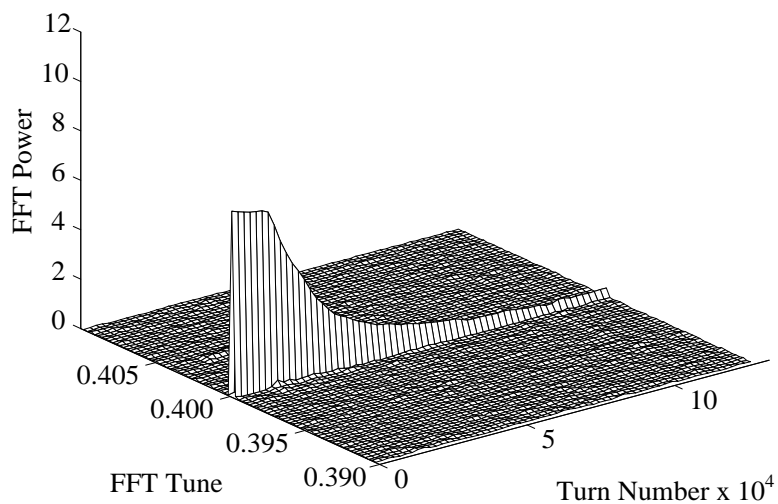


Figure 5.19: Same as Figure 5.15, with Q_M chirped from 200 to 250 Hz.

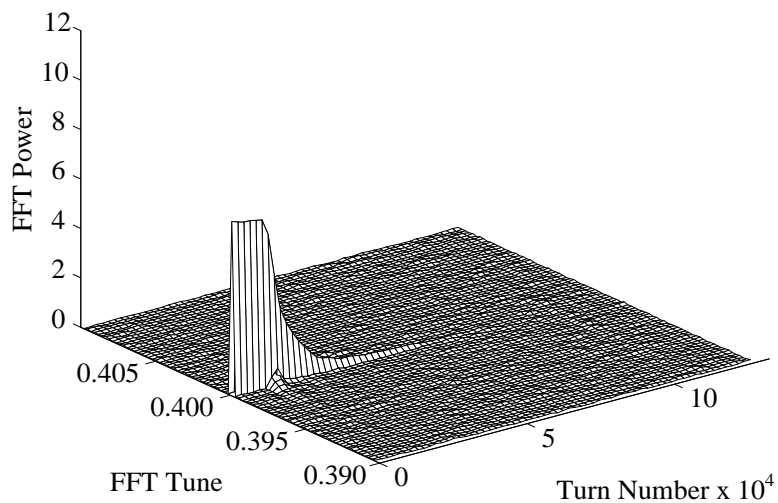


Figure 5.20: Same as Figure 5.15, with Q_M chirped from 250 to 300 Hz.

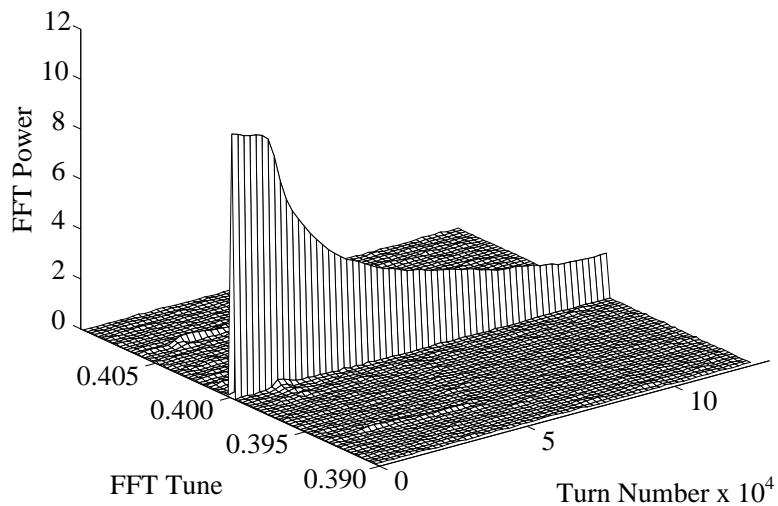


Figure 5.21: Same as Figure 5.15, with Q_M chirped from 300 to 350 Hz.

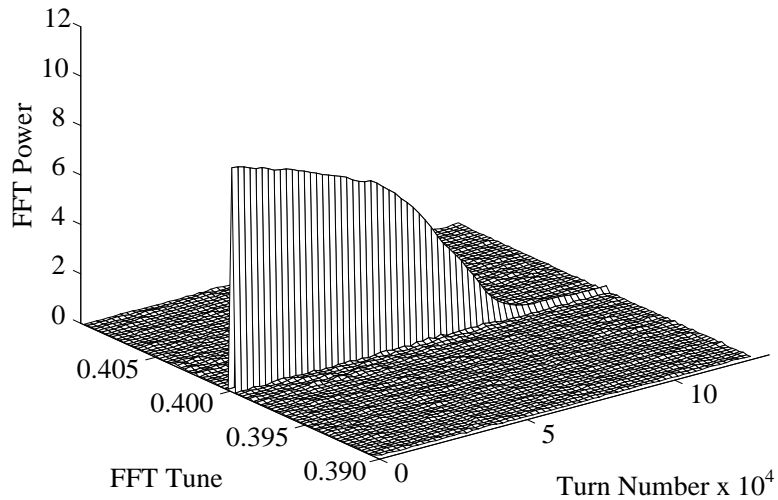


Figure 5.22: Same as Figure 5.15, with Q_M chirped from 0 to 350 Hz.

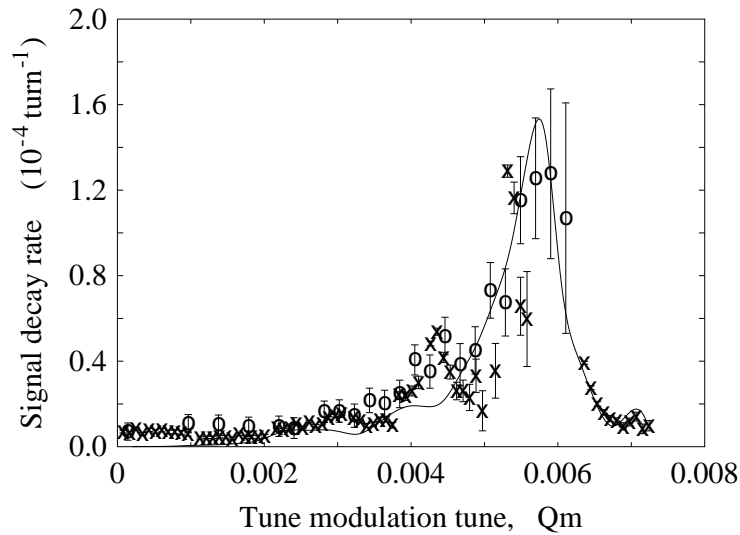


Figure 5.23: Persistent signal decay rate as a function of tune modulation frequency, Q_M in configuration 91_0. The tune modulation amplitude is held constant at $q = 2.04 \cdot 10^{-4}$. Circles represent experimental data from a single chirp from 0 to 350 Hz, and crosses represent data from seven individual 50 Hz scans. The line is a cubic spline fit through simulation data from the program OdChirp, with $Q_I = 6.3 \cdot 10^{-3}$.

The decay rate data for this modulation amplitude are shown in Figure (5.23), with crosses representing 50 Hz frequency chirps and circles representing the 350 Hz chirp. Error bars are produced by scaling the remaining persistent signal to the initial persistent signal, since a smaller signal size gives less accurate measures of the signal decay rate.

For larger modulation amplitudes in this data set, there was no sudden drop in decay rate indicating modulation above the island tune — each set of modulations destroyed the persistent signal at progressively smaller and smaller frequencies. A pair of these cutoff frequencies for higher modulation amplitudes are also shown in the tune modulation plane of Figure (5.24), just below the small-angle stability curve predicted by theory.

Another consistency with the results of Chapter 4 and simulation is the sudden

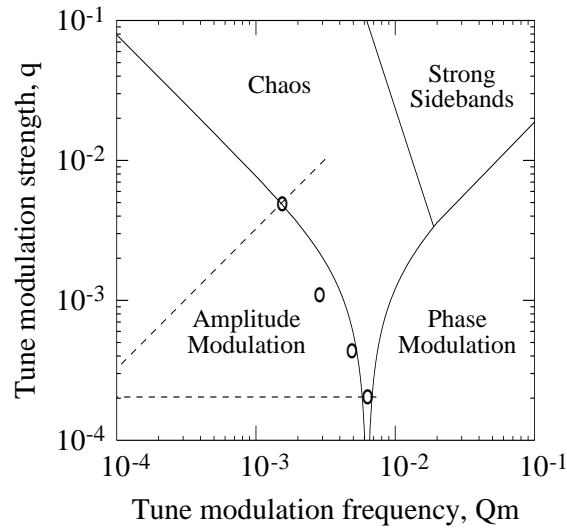


Figure 5.24: The tune modulation parameter plane, with stability lines as predicted by theory and experimental chirps for the 91_0 sextupole configuration. Q_1 has been set to the value $6.3 \cdot 10^{-3}$ here. The diagonal chirm corresponds to the data in Figure 5.11; the horizontal chirm corresponds to the 0 Hz to 350 Hz chirm shown in Figure 5.23.

stability at modulation frequencies above the island tune, as depicted in the Od-Chirm simulation results of Figure (4.4). The slowly rising response at frequencies lower than the island tune is also expected because the ensemble of particles filling the resonance island has a frequency distribution which is the same as that of an ensemble of stable pendula, varying from zero frequency at the separatrix to the island tune. Naively, little response is expected above the island tune, because there are no particles oscillating with this frequency to respond to the external drive. Another way to examine the island tune is to start the chirm above the island frequency and chirm downwards — a sudden sharp rise in response at the island tune should be observed. However, technical problems in the tune modulation controls prevented use of this sort of modulation during this experimental run.

5.4.3 Chirp Simulation and Comparison to Data

Simulations were performed of this modulated island system using the program OdChirp, which uses the tune modulation lattice of OdTrack and Odfp to simulate E778 conditions. This program launches an array of initial conditions, typically 10^3 , populating a transverse resonance island in much the same way resonance islands were populated to produce persistent signals in the experiment. After allowing untrapped particles to decohere over approximately 500 turns, tune modulation was applied in the exact same fashion as in the experimental run, with the same modulation ramps, strengths and frequencies. The turn-by-turn position of the centroid of the distribution of phase-locked particles was recorded.

This procedure allowed application of exactly the same data reductions as those applied to the actual data, and comparison of the simulated and actual frequency domain response. Because the island amplitude and base tune were well-defined from knowledge of the machine base tune and kicker settings, they could be inserted as known amplitudes, base tunes and octupole strengths for the simulation. The only free parameter then left in the simulation is the decapole strength; variation of this strength allowed a one-parameter fit to the data to produce a final value of the island tune, Q_I . An excellent fit was produced for an island tune $Q_I = 6.3 \cdot 10^{-3}$ or 296 Hz, in moderately good agreement with the predicted value of 335 Hz from particle tracking of the 91_0 lattice. Using this value of the island tune, a tune modulation plane can be drawn similar to Figure (4.1) showing excellent agreement for higher amplitude tune modulation chirps.